Appl. Phys. A (2016)122:337
DOI 10.1007/s00339-016-9872-6

Applied Physics A
Materials Science & Processing

Bipolar resistive switching and its temperature dependence in the composite structure of $BiFeO_3$ bilayer

W. J. Ma[1,2,3] · W. M. Xiong[1,2] · X. Y. Zhang[1,2] · Ying Wang[1,2] · H. Y. Zhang[1,2] · C. Q. Wang[1,2] · Biao Wang[1] · Yue Zheng[1,2]

Received: 6 August 2015 / Accepted: 15 November 2015

Abstract In order to demonstrate the control of $BiFeO_3$ thin film on the resistive switching effect and achieve the high-performance resistive switching device, the single layers and bilayer have been fabricated by chemical solution deposition method, respectively. In comparison with the single films, the composite film exhibits great performance of the resistive switching in endurance and repeatability, high stability and resistance ratio of high resistance state to low resistance state. Resistive switching effect in the $BiFeO_3$ composite structure demonstrates an effective way to improve the endurance and repeatability of the resistive switching characteristics by designing the relative devices.

W. J. Ma and W. M. Xiong have contributed equally to this work.

Electronic supplementary material The online version of this article (doi:10.1007/s00339-016-9872-6) contains supplementary material, which is available to authorized users.

✉ Yue Zheng
zhengy35@mail.sysu.edu.cn

Biao Wang
wangbiao@mail.sysu.edu.cn

[1] State Key Laboratory of Optoelectronic Materials and Technologies, School of Physics and Engineering, Sun Yat-sen University, Guangzhou 510275, China

[2] Micro&Nano Physics and Mechanics Research Laboratory, School of Physics and Engineering, Sun Yat-sen University, Guangzhou 510275, China

[3] Patent Examination Cooperation Center of the Patent Office, SIPO, Guangzhou 510535, China

1 Introduction

As the integrated circuit density rapidly increased in the last decades, the further miniaturization of modern nonvolatile memory devices is approaching the physical limit [1]. To solve the problem, many new memory mechanisms have been proposed, aiming to develop new high-density, fast-writing nonvolatile memory devices. Among those memory devices, resistive random access memory device (RRAM), with its simple metal–insulator–metal structure, high switching speed, outstanding scaling potential, is considered to be the most promising candidate for the next-generation nonvolatile memory device [2–6]. The nature of the resistive switching (RS) in RRAMs has been explored by various cutting-edge analysis techniques [7, 8]. The formation and rupture of the conductive filaments (CFs) in the RS materials have been proved to be responsible for the most of RS phenomena [9–12]. Based on this CF model, the mechanism of RS phenomenon can be described. For example, before the switching process, an electroforming operation is usually needed. The defects (usually the oxygen vacancies in oxides) move toward one of the electrodes under the electric field. As the defects accumulated, a CF is generated and bridged the insulator between two electrodes. The CF could be modified by applying opposite-polarity (bipolar) or different magnitude (unipolar) voltage, which induces the RS cell switching between high resistance state (HRS) and low resistance state (LRS).

Before being taken into application, there are several key concerns that need to be addressed in RRAMs, especially the RS repeatability and the endurance. The large fluctuation of RS parameters (e.g., V_{set} and V_{reset}, indicating the voltages of the resistance state switching from HRS to LRS and from LRS to HRS, respectively) makes it difficult to select the operation parameters, furthermore, causes the

Published online: 09 March 2016

operation window failure, and finally leads to poor endurance. According to the CF's mechanism, the large fluctuation of RS parameters in RRAMs probably comes from the uncontrolled rupture and repair of CFs. The random rupture and repair of CFs make the memory cell condition different from every cycle, thus leading to non-uniform RS characteristics [13]. If the rupture locations can be confined to a certain region, the RS uniformity could be significantly improved. Recently, our group reported highly uniform bipolar RS characteristics in $TiO_2/BaTiO_3/TiO_2$ multilayer RS cell [14]. The multilayer structure has been fabricated on $Pt/Ti/SiO_2/Si$ substrate by chemical solution deposition method. Highly uniform bipolar resistive switching (BRS) characteristics have been observed in $Pt/TiO_2/BaTiO_3/TiO_2/Pt$ cells. Analysis of the current–voltage relationship demonstrated that the space-charge-limited current conduction controlled by the localized oxygen vacancies should be important to the RS behavior. X-ray photoelectron spectroscopy results indicated that oxygen vacancies in TiO_2 play a crucial role in the RS phenomenon and the introduced $TiO_2/BaTiO_3$ interfaces result in the high uniformity of BRS characteristics.

$BiFeO_3$ is a perovskite-type multiferroic material, and its RS phenomenon has been observed [15–19]. Due to the abundant functional properties, $BiFeO_3$ has potential applications in developing multifunctional memory devices combining with ferroelectricity, ferromagnetism. However, the previous works [15–19] show that the pure $BiFeO_3$ thin films usually exhibit poor RS performance (i.e., poor resistance ratio of HRS and LRS, etc.) due to the large leakage current. Furthermore, it is believed that the boundary between composite structures of different crystal structures should affect the migration of oxygen vacancies and favor the controllable CF rupture [14]. The composite thin films may be considered crucial to the excellent BRS effect. In order to introduce a specific composite structure and find a simple method to significantly improve RS effect of $BiFeO_3$ thin film, in this work, RS characteristics have been explored in a bilayer composite structure, which is composed of TiO_2 and $BiFeO_3$, and fabricated on $Pt/Ti/SiO_2/Si$ substrate [19, 20]. Comparing with the $BiFeO_3$ or TiO_2 single-film RS devices, the stable resistances of RS effect and high resistance ratio of HRS and LRS in $BiFeO_3/TiO_2$ bilayer demonstrate controllable rupture and repair of CF in composite film RS device.

2 Experimental

As a demonstration, $BiFeO_3$ and $BiFeO_3/TiO_2$ films were deposited on $Pt/Ti/SiO_2/Si$ substrates by chemical solution deposition method as shown in Fig. 1a. TiO_2 precursor solution was prepared by dissolving titanium (IV) isopropoxide (Sinopharm, China, >98 %) in the mixture of acetic acid and ethanol. $BiFeO_3$ precursor solution was prepared by dissolving $Bi(NO_3)_3{\cdot}5H_2O$ (Sinopharm, China,

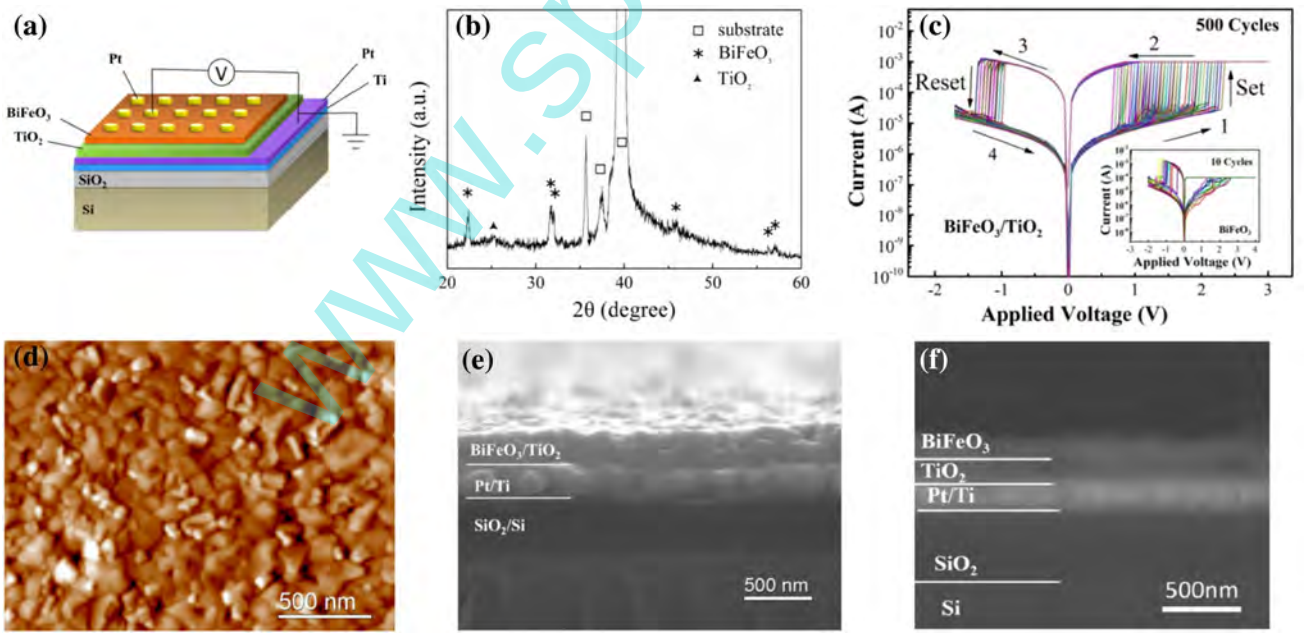

Fig. 1 **a** A schematic drawing of the measurement configuration. **b** XRD pattern of $BiFeO_3/TiO_2$ film. **c** The resistive switching *I–V* curves with consecutive cycles in $BiFeO_3/TiO_2$ RS cell. The sweep sequence is *marked* with the *numbers*. *Inset*: the RS *I–V* curve for $BiFeO_3$ single film with consecutive cycles. **d** Outmost surface AFM image, cross-sectional, **e** secondary electrons and **f** backscattered electrons images of the $BiFeO_3/TiO_2$ bilayer

>99 %) and $Fe(NO_3)_3{\cdot}9H_2O$ (Sinopharm, China, >98.5 %) in the mixture of 2-methoxyethanol and acetic acid. The volume ratio of 2-methoxyethanol and acetic acid is 4:1. The deposition of the films was carried out by spin coating at 4000 rpm for 50 s. Each layer was prefired at 350 °C to remove the organics. The samples were annealed at 600 °C for 2 h in the air atmosphere. Pt top electrodes with 0.2 mm in diameter were deposited on the films by ion sputtering with a shadow mask.

The crystallization of the films is confirmed by X-ray diffraction (XRD, Rigaku D-MAX 2200 VPC) with Cu Kα radiation ($\lambda = 0.154$ nm). The topography and cross-sectional images of the films were examined by atomic force microscopy (AFM, CSPM5000) and scanning electron microscopy (SEM, FEI Quanta 400F), respectively. Chemical state and depth profile of $BiFeO_3/TiO_2$ bilayer were obtained by X-ray photoelectron spectroscopy (XPS, ESCA LAB 250). The electrical properties were measured with Keithley 4200 semiconductor characterization system.

3 Results and discussion

Results in Fig. 1b, d–f show crystallization, topography, cross-sectional secondary electrons (SE) and backscattered electrons (BSE) images of the $BiFeO_3/TiO_2$ bilayer structure, respectively. Figure 1b exhibits the XRD spectrum of $BiFeO_3/TiO_2$ film deposited on the $Pt/Ti/SiO_2/Si$ substrate. The diffraction peaks of $BiFeO_3$ are clearly observed. In contrast, the TiO_2 peaks are barely detected, probably owing to blocking effect of $BiFeO_3$ layer. In order to confirm the $BiFeO_3/TiO_2$ bilayer structure, the element distribution along the depth direction has also been studied by X-ray photoelectron spectroscopy (XPS) with the Ar^+ sputtering in following section, which confirms existence of the TiO_2 layer in the bilayer. The surface and cross-sectional morphology of $BiFeO_3/TiO_2$ film are studied by AFM and SEM, respectively, and the results are shown in Fig. 1d–f. The measurement configuration is depicted in Fig. 1a. Before the RS measurement, an electroforming process is usually needed (See Fig. S1). During the forming process, high electric field drives oxygen vacancies moving toward the cathode, inducing a CF growth from the cathode to the anode. Figure 1c shows the *I–V* curves with more than 500 consecutive RS cycles in semilog scale, and inset is the RS *I–V* curves for $BiFeO_3$ single film with ten consecutive cycles. The voltage is swept in the sequence of 0 V → 3 V → 0 V → −1.7 V → 0 V, with steps of 0.05 V. The set process occurs in the voltage sweep 0 V → 3 V, resulting in a sudden current increase, and switches the resistance state from HRS to LRS. A compliance current of 1×10^{-3} A is adopted to avoid the permanent dielectric breakdown. Then, the voltage sweeps reversely, and the reset process can be observed in the negative-voltage region. More than 500-cycle RS loops exhibit high repeatability and stability, which *I–V* curves in HRS and LRS are highly overlapped. Furthermore, the critical voltage V_{set} and V_{reset} are concentrated in the narrow voltage regions of 0.7–2.5 and −1.4 to −1 V, respectively. In order to give reference, XRD patterns,

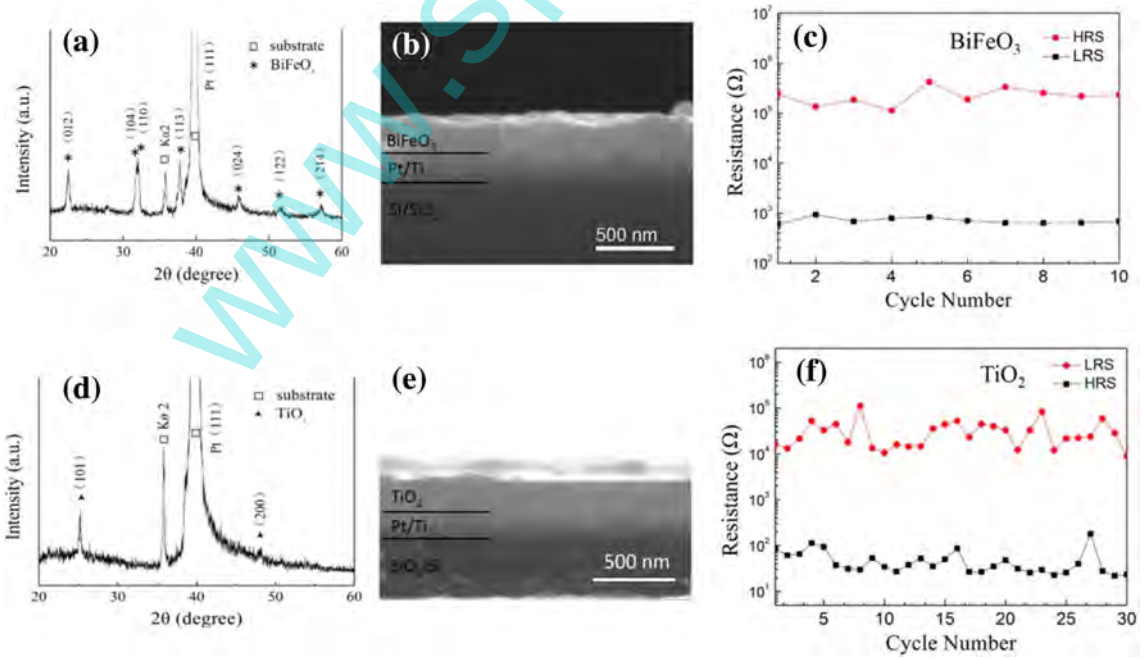

Fig. 2 XRD pattern, cross-sectional SEM image and HRS/LRS of $BiFeO_3$ and TiO_2 single film

cross-sectional SEM images and RS effects of the $BiFeO_3$ and TiO_2 single films are also studied as shown in Fig. 2. The endurance for $BiFeO_3$ single film fabricated by chemical solution deposition method is about 10-cycle as shown in Fig. 2c. Besides that, poor repeatability of switching curves also can be observed (especially the curves in HRS). Comparing the RS performances of $BiFeO_3/TiO_2$ film with those of $BiFeO_3$ single film, it is clear that the composite film shows overwhelming advantage in endurance and repeatability. It confirms the view that the composite structure can greatly improve the performance of RS devices.

Results of Fig. 3 show the distribution of V_{set}/V_{reset} and the resistance evolution of $BiFeO_3/TiO_2$ bilayer in the RS cycles, which reconfirm the great repeatability of the memory cell. As shown in Fig. 3a, the distribution of V_{reset} and V_{set} is ranged in -1 to -1.4 and 0.7–2.5 V, respectively. It should be noticed that nearly 90 % of the V_{reset} values concentrate in 1–1.1 V and 80 % of the V_{set} values concentrate in 1.1–1.45 V. The narrow distribution of V_{reset} and V_{set} indicates the stable rupture and repair of the CF in $BiFeO_3/TiO_2$ RS cell. In addition, the small value of V_{set} and V_{reset} benefits to reducing the power consumption. Figure 3b exhibits the resistance evolution in HRS and LRS in the RS cycles, all of the resistance values are read in -0.1 V. The values of R_{HRS} and R_{LRS} are maintaining in

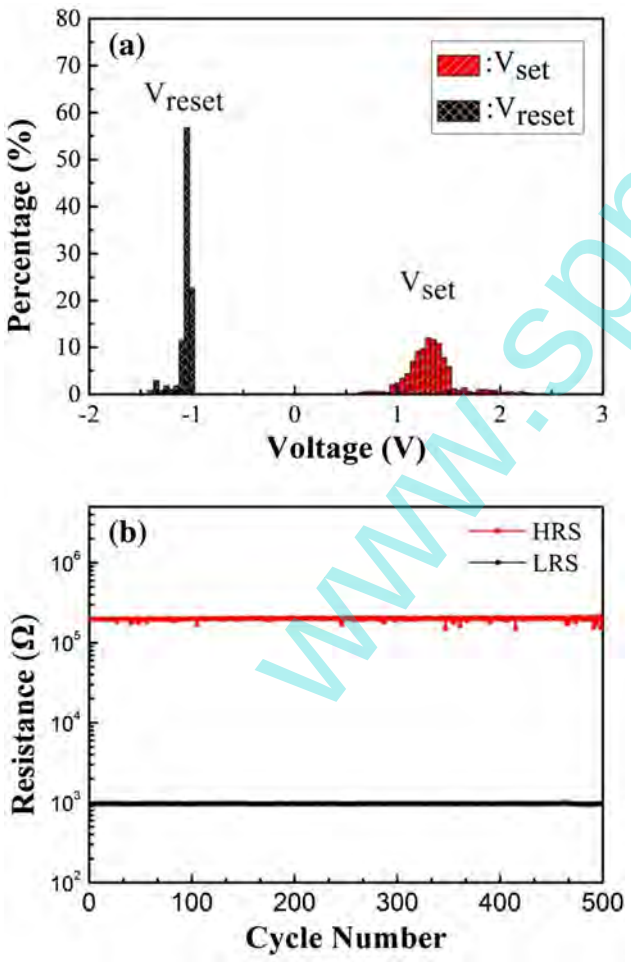

Fig. 3 **a** Distribution of V_{set} and V_{reset} and **b** resistance evolution of HRS and LRS (the resistance values are read in -0.1 V)

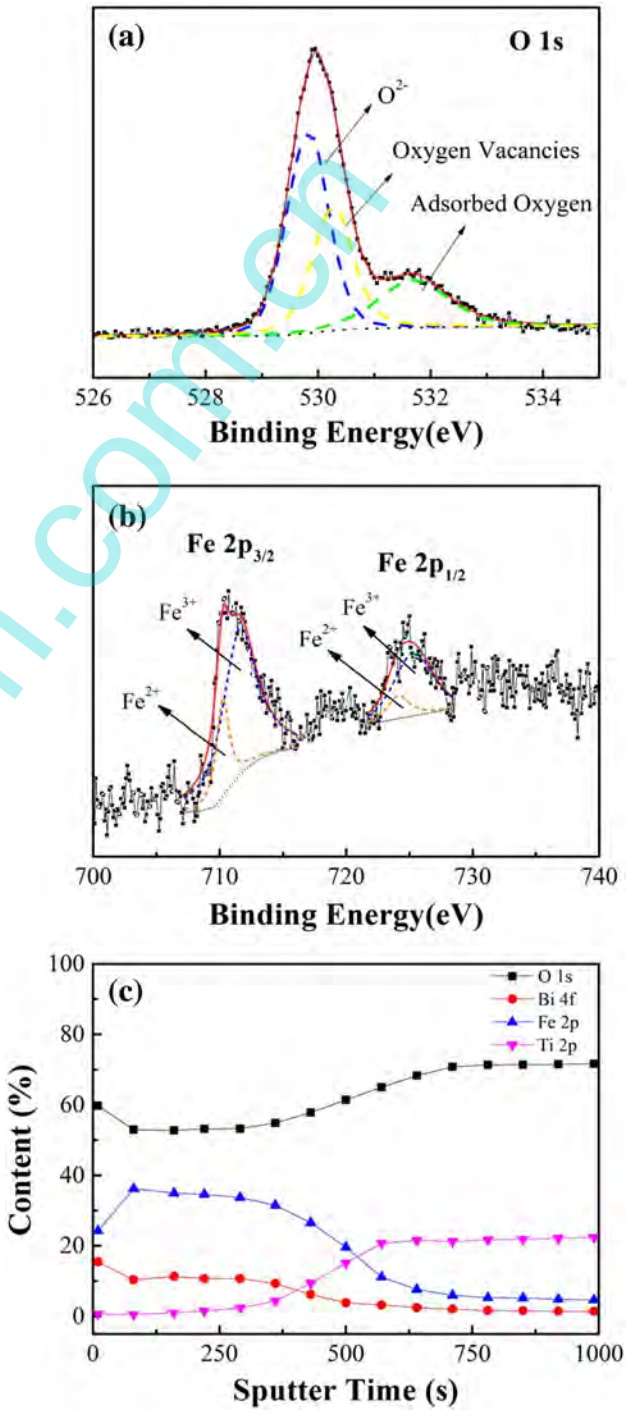

Fig. 4 **a** XPS spectra of O1*s* and **b** Fe 2*p* on the outmost of $BiFeO_3/TiO_2$ film. **c** Elemental depth profile acquired by XPS with the help of Ar^+ sputtering

200 KΩ and 1 KΩ, without any decaying. Comparing with the $BiFeO_3$ or TiO_2 single-film RS devices (Fig. 2c, f), the extremely stable R_{HRS} and R_{LRS} in $BiFeO_3/TiO_2$ bilayer demonstrate controllable rupture and repair of CF in composite film RS device. In addition, the resistance ratio, R_{HRS}/R_{LRS}, is as high as 200, which is much higher than the results of single-layer $BiFeO_3$ thin films in previous works [15–19].

As we have mentioned above, oxygen vacancies are crucial for RS phenomenon. Here, the existence of oxygen vacancies is confirmed by XPS. Figure 4a, b is the O1*s* and Fe 2*p* XPS spectra detected on the $BiFeO_3/TiO_2$ outmost surface, respectively. As shown in Fig. 4a, O1*s* XPS data could be resolved into three Gaussian peaks centered in 529.8, 530.6 and 531.7 eV, which are assigned to lattice oxygen, oxygen vacancies and adsorbed oxygen, respectively. It should be noticed that the peak of oxygen vacancies takes up a considerable part of total peak area, indicating a large amount of oxygen vacancies exists in the $BiFeO_3$ layer. Figure 4b exhibits two broad peaks of Fe $2p_{3/2}$ and Fe $2p_{1/2}$, which demonstrate the coexistence of Fe^{3+} and Fe^{2+} valence states. The deconvolution of the data indicates the Fe^{3+} $2p_{3/2}$ and Fe^{3+} $2p_{1/2}$ peaks are in 711.8 and 725.3 eV; additionally, the Fe^{2+} $2p_{3/2}$ and Fe^{2+} $2p_{1/2}$ are in 710.2 and 724.1 eV, respectively. The coexistence of Fe^{3+} and Fe^{2+} is coincident with the oxygen vacancies peak in Fig. 4b. According to the defect chemistry, the variation in Fe valence state from Fe^{3+} to Fe^{2+} is owing to the charge compensation of oxygen vacancies. The element distribution along the depth direction has also been studied by XPS with the Ar^+ sputtering. The depth profile is presented in Fig. 4c, which confirms the bilayer structure of $BiFeO_3/TiO_2$ film. However, Ar^+ bombardment will change the chemical state of some compounds [21]. For example, the valence of Ti in TiO_2 will be reduced to Ti^{3+} or Ti^{2+} after Ar^+ bombardment. In our experiment, the XPS chemical state analysis of TiO_2 layer (not shown in the paper), which is obtained after Ar^+ bombardment, is not available. Nevertheless, it is supposed that there are a large number of oxygen vacancies in the TiO_2 layer, for its famous oxygen-deficient nature. Furthermore, the view that oxygen vacancies migration causes the RS has been generally accepted.

In order to gain insight into the CF formed in $BiFeO_3/TiO_2$ composite thin film, temperature-dependent *I–V* curves in HRS and LRS were measured. To avoid

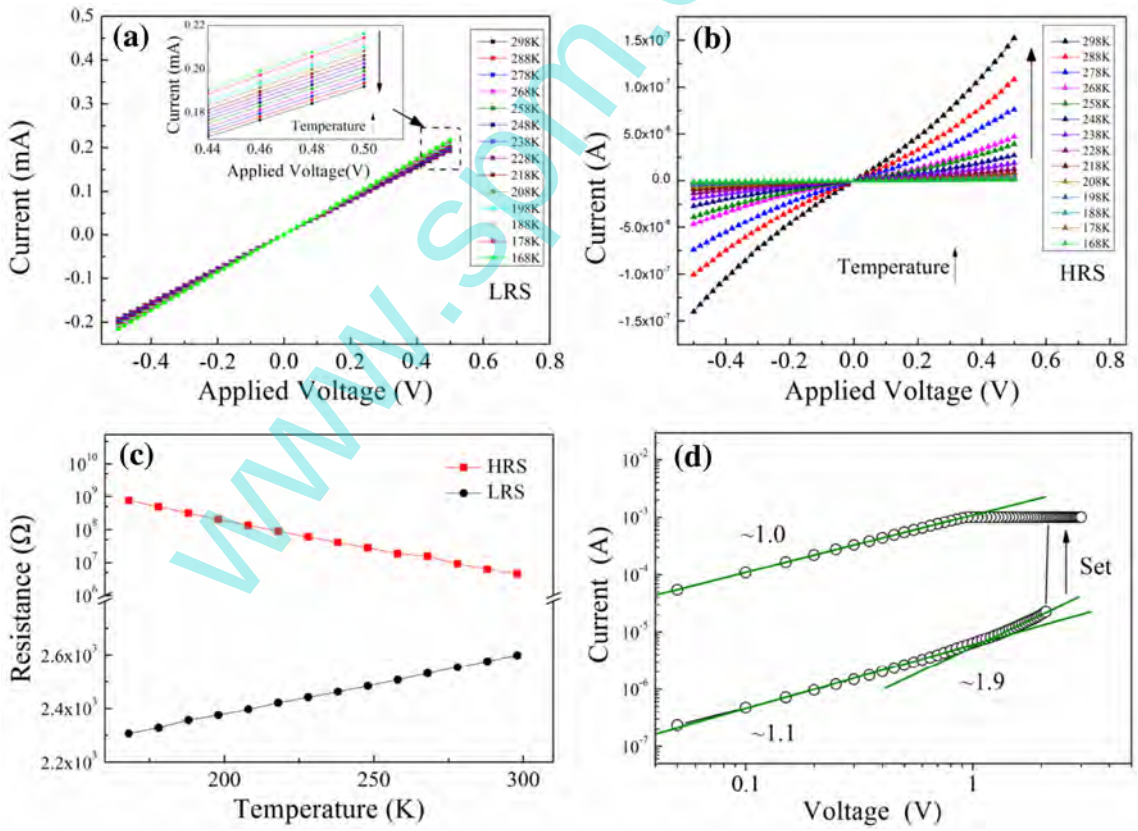

Fig. 5 **a**, **b** Temperature-dependent *I–V* curves in LRS and HRS. Temperature range: 168–298 K. Voltage range: −0.5–0.5 V. **c** Temperature-dependent resistance for LRS and HRS (the resistance values are read in −0.1 V). **d** The linear fitting for the *I–V* curves in double-logarithmic scale, and the corresponding slopes for each part

resistance switching, the test voltage range is confined in −0.5 to 0.5 V. Figure 5a, b presents the temperature-dependent *I–V* curves for HRS and LRS in the temperature range of 168–298 K. It can be seen that the *I–V* curves regularly varied with the increase in temperature. For the LRS, the current decreases as the temperature increases. In contrary, the current in the HRS increases with the increase in temperature. The dependence of resistance on temperature for both HRS and LRS has been redrawn in Fig. 5c (the resistances are read in −0.1 V). The monotonous increasing and decreasing tendencies in the temperature-dependent resistance for LRS and HRS demonstrate the metallic behavior of the CF and the semiconducting behavior of matrix, respectively. It is generally accepted that CF can be regarded as the oxygen vacancy chain. As we know, oxygen vacancy, which acted as donor, can reduce the oxide, favor the reconstitution of the local region, and lead to the insulator-to-metal transition. For the TiO_2, Magnéli phases (Ti_nO_{2n-1}, $n = 2, 3, 4$) conductive channels, which exhibit metallic behavior, have been directly observed in both unipolar [8] and bipolar [22] RRAMs. Similarly, oxygen vacancies chains could also reduce the Fe^{3+} to Fe^{2+} in the vicinity, cause the structure distortion, and give rise to a metallically conductive path [23].

To further understand the conduction mechanism, the typical *I–V* data have been fitted to several conduction models. The best fittings are shown in Fig. 5d, in which the *I–V* relation is plotted in double-logarithmic scale and the fitting results are highlighted in green line. For HRS, the *I–V* relation can be divided into two regions, 0–1.1 and 1.1–2.1 V, in which the slope of curves are 1.1 and 1.9, respectively. This accords with the space-charge-limited current (SCLC) conduction. In the low-voltage region (0–1.1 V), the cell exhibits Ohmic behavior ($I \propto V$). When the voltage increases, large amount of excess injected carriers accumulates to forming a space-charge area, block the following charge injection, and lead to the nonlinear *I–V* relation ($I \propto V^2$). For LRS, the linear *I–V* relation with the slope of 1.0 confirms the Ohmic behavior.

4 Conclusion

In conclusion, we have proposed a $BiFeO_3/TiO_2$ composite structure to achieve high-performance RS memory device. As a demonstration, $BiFeO_3$, TiO_2 and $BiFeO_3/TiO_2$ films were fabricated and measured. In comparison with the $BiFeO_3$ single film, the $BiFeO_3/TiO_2$ composite film exhibits great performance in endurance and repeatability. Comparing with the $BiFeO_3$ or TiO_2 single-film RS devices, the extremely stable R_{HRS} and R_{LRS} in $BiFeO_3/TiO_2$ bilayer demonstrate controllable rupture and repair of CF in composite film RS device. In addition to the stability, the resistance ratio, R_{HRS}/R_{LRS}, is as high as 200, making it easy to distinguish the memory states. XPS and temperature-dependent *I–V* tests confirm that oxygen vacancies-based metallic CF form in $BiFeO_3/TiO_2$ RS cell. Great RS effect in the bilayer composite demonstrates a great effective way to improve the RS endurance and repeatability of $BiFeO_3$ by designing the composite thin film of the devices.

Acknowledgments We acknowledge the financial support of the National Natural Science Foundation of China (NSFC) (Nos. 51172291, 11474363, 11372361). Yue Zheng also thanks support by the Fundamental Research Funds for the Central Universities, NCET in University, Research Fund for the Doctoral Program of Higher Education, Fok Ying Tung Foundation, Science and Technology Innovation Project of Guangdong Provincial Education Department, Guangdong Natural Science Funds for Distinguished Young Scholar and China Scholarship Council.

References

1. Y. Fujisaki, Review of emerging new solid-state non-volatile memories. Jpn. J. Appl. Phys. **52**, 040001 (2013)
2. A. Sawa, Resistive switching in transition metal oxides. Mater. Today **11**, 28 (2008)
3. R. Waser, M. Aono, Nanoionics-based resistive switching memories. Nat. Mater. **6**, 833 (2007)
4. R. Waser et al., Redox-based resistive switching memories-nanoionic mechanisms, prospects, and challenges. Adv. Mater. **21**, 2632 (2009)
5. G. Chen et al., Resistive switching and magnetic modulation in cobalt-doped ZnO. Adv. Mater. **24**, 3515 (2012)
6. Z. Yan et al., High-performance programmable memory devices based on Co-doped $BaTiO_3$. Adv. Mater. **23**, 1351 (2011)
7. M.H. Lee, C.S. Hwang, Resistive switching memory: observations with scanning probe microscopy. Nanoscale **3**, 490 (2011)
8. D.H. Kwon et al., Atomic structure of conducting nanofilaments in TiO_2 resistive switching memory. Nat. Nanotech. **5**, 148 (2010)
9. M.J. Lee et al., A fast, high-endurance and scalable non-volatile memory device made from asymmetric Ta_2O_{5-x}/TaO_{2-x} bilayer structures. Nat. Mater. **10**, 625 (2011)
10. K.M. Kim, D.S. Jeong, C.S. Hwang, Nanofilamentary resistive switching in binary oxide system; a review on the present status and outlook. Nanotechnology **22**, 254002 (2011)
11. J.Y. Son, Y.H. Shin, Direct observation of conducting filaments on resistive switching of NiO thin films. Appl. Phys. Lett. **92**, 222106 (2008)
12. S.B. Long et al., Voltage and power-controlled regimes in the progressive unipolar RESET transition of HfO_2-based RRAM. Sci. Rep. **3**, 2929 (2013)
13. J.H. Yoon et al., Highly improved uniformity in the resistive switching parameters of TiO_2thin films by inserting Ru nanodots. Adv. Mater. **25**, 1987 (2013)
14. W.J. Ma et al., Highly uniform bipolar resistive switching characteristics in $TiO_2/BaTiO_3/TiO_2$ multilayer. Appl. Phys. Lett. **103**, 262903 (2013)
15. K. Yin et al., Resistance switching in polycrystalline $BiFeO_3$ thin films. Appl. Phys. Lett. **97**, 042101 (2010)

16. T.L. Qu et al., Resistance switching and white-light photovoltaic effects in $BiFeO_3$/Nb–$SrTiO_3$ heterojunctions. Appl. Phys. Lett. **98**, 173507 (2011)
17. C. Wang et al., Switchable diode effect and ferroelectric resistive switching in epitaxial $BiFeO_3$ thin films. Appl. Phys. Lett. **98**, 192901 (2011)
18. R. Chen et al., Uniform bipolar resistive switching behaviors in $BiFeO_3$ thin films on Fe-doped $LaNiO_3$ electrodes. Appl. Phys. Express **7**, 095801 (2014)
19. Y. Shuai et al., Nonvolatile bipolar resistive switching in Au/$BiFeO_3$/Pt. J. Appl. Phys. **109**, 124117 (2011)
20. K. Szot et al., TiO_2—a prototypical memristive material. Nanotechnology **22**, 254001 (2011)
21. S. Hashimoto et al., Formulation for XPS spectral change of oxides by ion bombardment as a function of sputtering time. Surf. Sci. **556**, 22 (2004)
22. J.P. Strachan et al., Direct identification of the conducting channels in a functioning memristive device. Adv. Mater. **22**, 3573 (2010)
23. J.M. Luo et al., Nonpolar resistive switching in Mn-doped $BiFeO_3$ thin films by chemical solution deposition. Appl. Phys. Lett. **101**, 062902 (2012)